THE SIZE AND POSITION OF THE X-RAY SOURCE IN THE CRAB NEBULA

M. ODA, H. BRADT, G. GARMIRE, G. SPADA,
B. V. SREEKANTAN, H. GURSKY,
R. GIACCONI, P. GORENSTEIN,
AND J. R. WATERS

THE SIZE AND POSITION OF THE X-RAY SOURCE IN THE CRAB NEBULA

During a recent rocket flight, we observed the 1–6 keV X-radiation from the Crab Nebula with a modulation collimator of high resolution. We find the emission region to be centered on the Crab and of finite size. These results are in agreement with those of the lunar occultation experiment carried out by Bowyer, Byram, Chubb, and Friedman (1964). The present measurement improves upon the earlier work in that it provides size and position information along two nearly perpendicular directions rather than the one direction of the lunar transit. Also, since the measurements of Sco X-1 (Gursky, Giacconi, Gorenstein, Waters, Oda, Bradt, Garmire, and Sreekantan 1966*a*, *b*) and the Crab Nebula were made with the same instrument during a single flight, we were able to directly observe the qualitatively different appearance in X-rays of a starlike source (Sco X-1) and a source of finite angular size (Crab).

The Crab Nebula was first positively identified as a strong X-ray source by the above-mentioned occultation experiment. Thus the Crab is now known to be bright in a frequency range from 10^7 to 10^{19} c/s. In the radio and optical regions, the radiation is believed to be synchrotron emission because of the observed high degrees of polarization. Although it has been argued that the observed X-rays represent an extension of the synchrotron radiation to higher energies (Woltjer 1964; Shklovskii 1966), there is no conclusive evidence that eliminates other possibilities, notably thermal emission from a hot plasma. Arguments in support of this latter mechanism have recently been presented by Morrison and Sartori (1967). In any case, the gross dynamics of the Crab Nebula must be affected in a significant way by the X-ray emission since the total radiated power in X-rays is comparable to that at optical wavelengths and greatly exceeds that at radio wavelengths. Thus, comparison of the detailed angular structure in the X-ray, optical, and radio regions should contribute materially toward our understanding of the Crab Nebula.

The data reported here were obtained during a sounding rocket flight on March 8, 1966. Observations of the bright X-ray source in Scorpio, Sco X-1, during the same flight yielded both a 20″ upper limit to its angular size and its position to a precision of 4 sq. arc min (Gursky *et al.* 1966*a*, *b*) which, in turn, made possible an identification of its optical counterpart (Sandage, Osmer, Giacconi, Gorenstein, Gursky, Waters, Bradt, Garmire, Sreekantan, Oda, Osawa, and Jugaku 1966). Both the Crab and Scorpio observations were made with the same optical X-ray sensor system. It consisted of proportional counters with 50-μ Be windows and 30 mg/cm^2 of xenon, a camera, and two four-grid modulation collimators, each with multiple 40″ × 10° (FWHM) angular transmission zones, or "bands," separated one from another by about 5′. These angular dimensions differed for the two (one "long" and one "short") collimators by about 5 per cent to provide a vernier effect which in principle permits one to identify the angular transmission band corresponding to a given peak in the X-ray data. The 16 mm camera took successive 1-sec exposures and simultaneously viewed a 12° × 8°.5 star field and a portion of each collimator. The collimators were illuminated by a diffuse light source in such a way that the X-ray transmission bands were imaged directly onto the image of the star field. This allowed us to project lines of position corresponding to each data peak directly onto the celestial sphere. The entire detection system viewed the sky through the front end of the Aerobee 150 rocket.

The observations were made in the following way. The rocket was pointed toward the Crab Nebula for a period of about 40 sec during which the jitter in the attitude control

system caused the rocket to scan the Nebula at rates of several arc minutes per second. Directly following this sequence, the rocket was rolled 60° about its long axis, and a 40-sec "postroll" period provided data which yielded lines of position on the celestial sphere which cross at 60° those obtained during the "preroll" period. During the preroll and postroll periods there were, respectively, nine and four transits of the optical Crab by the transmission bands of the short collimator. The long collimator made, respectively, nine and five transits during these periods.

The individual transits of the source did not appear as statistically significant peaks in the counting-rate data. Therefore, the optical aspect data, precise to 15″, were used to sum the data from the successive transits of the source region. For both the short and

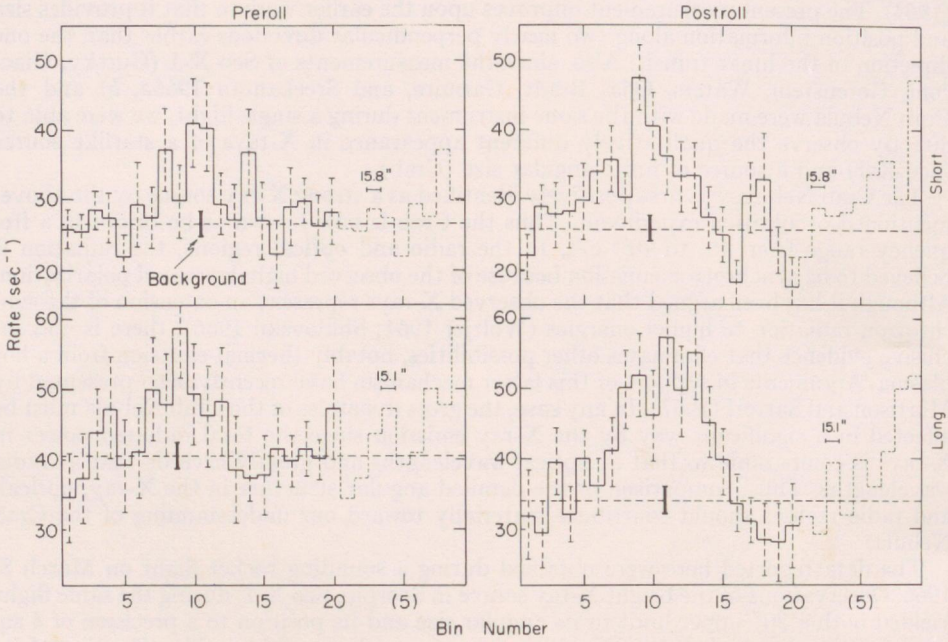

FIG. 1.—Data after initial superposition with periodicity equal to the angle of separation between adjacent transmission directions, namely, 5′1.″91 and 5′16.″62 for the long and short collimators, respectively. These angular intervals are divided into 20 equal bins and, in each histogram, the center of bin 10 represents the Becvar coordinates for the center of the Crab Nebula.

long collimators, the angular interval between two successive transmission bands was divided into 20 equal bins, each of approximately 15″ width. Both systems of 20 bins were fixed upon the celestial sphere, essentially superimposed, with bin 10 centered at (1950.0) $\alpha = 5^h31^m30^s$, $\delta = 21°59'$, the coordinates listed in the Becvar catalogue for the center of the Crab Nebula. In order to reduce the effects of background counts, we restricted the energy region studied to 1–6 keV. Each detected X-ray was credited to the bin which at that moment was being traversed by the center of a collimator transmission band. Also, the total time spent in each bin was accumulated. This superposition was carried out separately for each of the two collimators ("short" and "long") for both the preroll and postroll periods. The resultant rates with statistical errors are presented in Figure 1.

The centroid of the peak in each of the four sets of data in Figure 1 lies close to bin 10. Thus, in both scan directions, the center of the X-ray source lies close to the center of the

Crab. We further note that the occurrence of the "long" and "short" peaks at the same bin number eliminates from consideration most of the other celestial positions which, due to the multiplicity of transmission directions through the collimator, might be candidates for the location of the X-ray source. The background rates indicated in Figure 1 with their statistical errors were calculated from the rates in the 8 or 9 bins most removed from the peak. In each case they are consistent with the rates of about equivalent statistical significance obtained during the gross maneuvers of the rocket prior to and subsequent to the Crab observations.

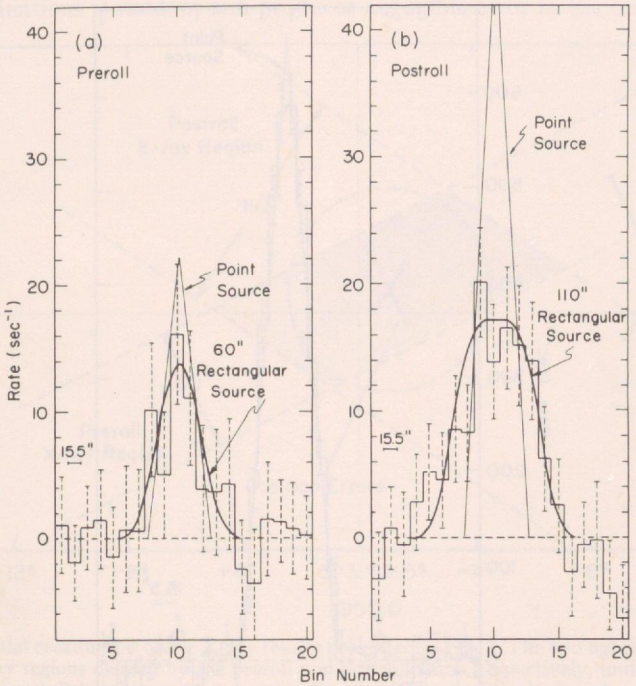

FIG. 2.—Summation of all data obtained during the preroll (postroll) hold on the Crab Nebula, plotted with background subtracted as a function of bin number. The error bars indicate one standard deviation and include the effect of the uncertainty in the background rates. The bin width (15.″46) is the mean of the long and short bin widths. The expected responses for point and rectangular source distributions are also presented.

In order to obtain celestial positions and angular sizes based on the entire data we superimposed the short and long data bin by bin for both the preroll and postroll observations (Fig. 2). Since the angular sizes of the long and short bins are different by 5 per cent, the straightforward bin-by-bin superposition smears the angular resolution, but at most by 7″ ($\frac{1}{2}$ bin) in bin 1 and bin 20. The effect on the rates is negligible. In Figure 2 we also show the expected responses with normalized areas of point sources and of rectangular sources of uniform intensity which best fit the data. In the case of the preroll data the most probable angular size is 60″ $\pm$ 60″ for the assumed rectangular shape. However, we cannot exclude a point source. During the postroll period the source spent a greater fraction of the time within the 40″ transmission zones. The data are therefore of better quality and yield an angular size of 110″ $\pm$ 25″. In this case a point source is clearly excluded. The quoted errors are based upon χ^2 tests of other source sizes and represent a probability of occurrence equal to that expected for 1 standard deviation in a

normal distribution. As we will discuss later, these data are also consistent with an X-ray source region identical in shape and size to that of the optical source.

The total counting rates due to the source in the 1–6 keV region are 1.1 ± 0.3 cm^{-2} sec^{-1} and 2.1 ± 0.3 cm^{-2} sec^{-1} for the preroll and postroll data, respectively. These rates include the effects of the limited angular aperture (40″ FWHM) of the collimators and the reduction of effective counter area by the X-ray shadows of the collimator, grid, and counter-window support structures. The stated precision in these rates is statistical and arises, in part, from the statistical errors in the background measurements. The apparent

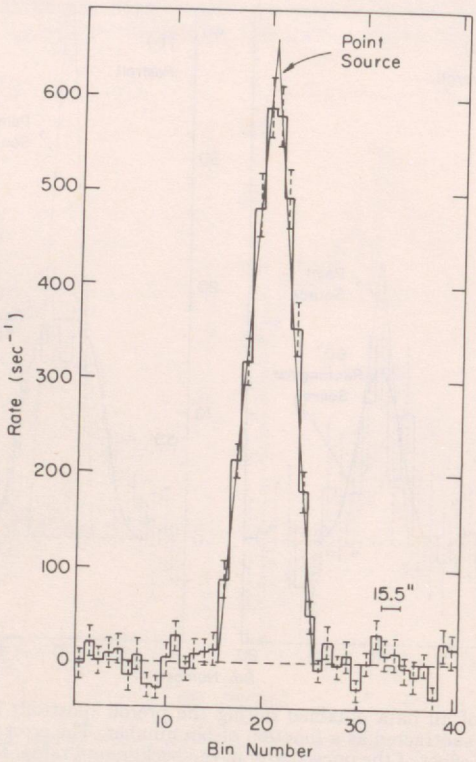

FIG. 3.—Superposition of all data obtained during "hold" portion ($289 < t < 302$ sec) of the Sco X-1 observations described by Gursky *et al.* (1966*a*, *b*).

discrepancy in the rates can be understood either as a statistical fluctuation in their difference of two standard deviations or as systematic errors in our initial assumptions as to which bins in Figure 1 represent true measurements of the background. We have found, however, that our conclusions regarding the size and location of the source are not significantly affected by the assumption of any other set of background levels which is compatible with the flight data.

To test this method of analysis we have carried out the same superposition techniques on the Sco X-1 data obtained later in the same flight (Fig. 3). The data indeed conform to a point source with a precision of about 15″, and, as previously reported, the line of position corresponding to the centroid of the peak lies within 20″ of the optical object Sco X-1.

The celestial position of the center of the Crab X-ray source is obtained from the

intersection of the lines of position corresponding to the centroids of the peaks in Figure 2:

$$\alpha(1950.0) = 5^h31^m30^s ,$$

$$\delta(1950.0) = 21°59'.1 .$$

The statistical errors (standard deviation) in the centroid determinations are 20″ and 15″ in the preroll and postroll data, respectively. The 15″ error in each of the many aspect determinations is random and produces negligible error in the centroid position.

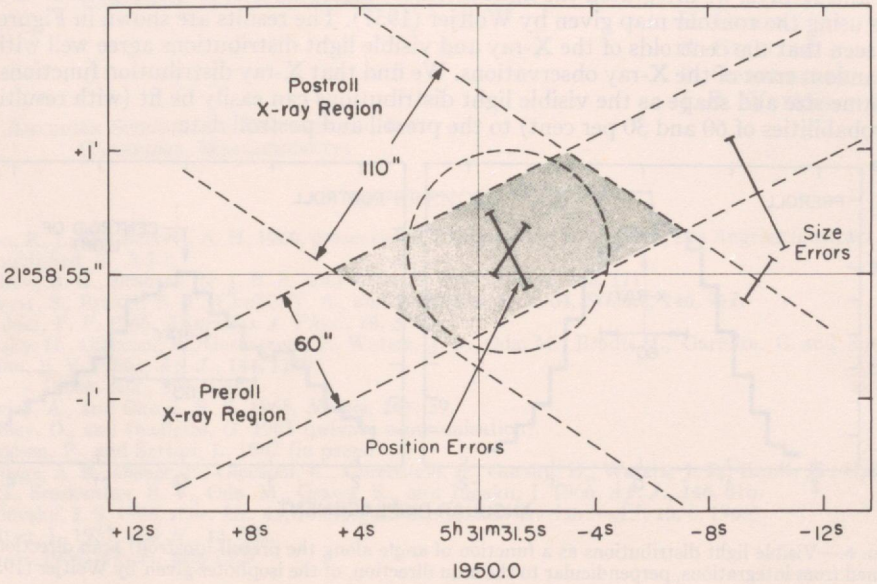

FIG. 4.—Celestial coordinates of the X-ray results presented in Fig. 2. The two lightly shadowed bands indicate the X-ray regions defined by the preroll and postroll scans, respectively, under the assumption of rectangular source distributions in each scan direction. The darkly shadowed area of intersection indicates the most probable X-ray source region under these assumptions. The error bars represent the statistical errors; the systematic errors in the position are estimated to be less than 15″. The size and shape of the source are idealized as a circular area of diameter 100″. The origin of the coordinate system is the southwest component of the central double star.

We previously estimated (Gursky *et al.* 1966*b*) that a systematic error of as much as 30″ could be introduced by uncertainties in the correlation of the optical fiducial pattern with the X-ray transmission directions and, probably more important, by errors in extrapolation across the film. We now believe that systematic errors for the Crab are somewhat smaller because (1) the discrepancy between the position of the optical object Sco X-1 and the position deduced from the flight data was, as mentioned above, only about 20″ and (2) the position of the Crab lay closer to the center of the field of view than did Sco X-1.

The position and size results from this experiment are presented schematically in Figure 4. The darkly shaded area represents the most probable X-ray source region. Because of the large statistical error in the preroll size result, we choose to report the circular area as an idealization of the size and shape of the X-ray source. Its diameter (100″) is obtained from a statistical weighting of the preroll and postroll data.

In Figure 5 (Plate L1) we have transferred these results to a Palomar photograph of

the Crab Nebula. The earlier results based on the occultation experiment are also shown. The dashed line, marked *NRL*, gives the originally reported (Bowyer *et al.* 1964) position of the lunar limb corresponding to the observed peak of the X-ray distribution. Manley and Ouellette (1965) have recently recalculated the lunar position taking into account parallax introduced by the rocket motion during the flight and their result is the solid line marked *NRL*. The effect of this parallax was to cause the limb of the Moon to almost double its rate of traversal across the Crab, and this, in turn, gives rise to an angular size of about 2′ rather than about 1′ as originally reported.

In order to make a more quantitative comparison between the distribution of visible light and X-rays, we integrated the light intensity in the directions normal to our X-ray scans using the contour map given by Woltjer (1957). The results are shown in Figure 6. It is seen that the centroids of the X-ray and visible light distributions agree well within the random error of the X-ray observations. We find that X-ray distribution functions of the same size and shape as the visible light distributions can easily be fit (with resulting χ^2 probabilities of 60 and 30 per cent) to the preroll and postroll data.

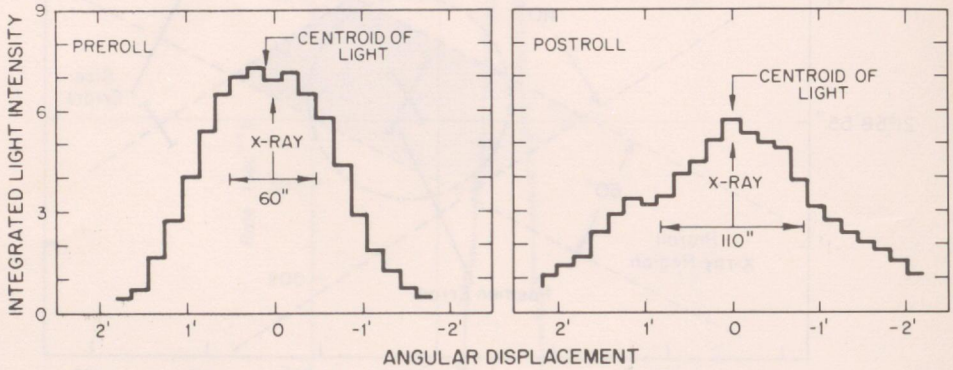

FIG. 6.—Visible light distributions as a function of angle along the preroll (postroll) scan direction as obtained from integrations, perpendicular to the scan direction, of the isophotes given by Woltjer (1957). The X-ray results are taken from Fig. 2.

In summary, this experiment yields two principal results. First, the X-ray and visible light distributions have a common center within the 15″ precision of the measurement. Second, the source has a finite angular extent. The data are consistent with X-ray emission regions which range in size and shape from uniform emission by the central two arc minutes of the Crab to a distribution identical to that of the visible light. These results place constraints upon the details of the possible models for X-ray emission. For instance, the markedly off-center features of the Crab, such as the maximum of the radio polarization at centimeter wavelengths (Gardner 1965; Allen and Barrett 1966) or the small diameter radio source at 25–40 mc/s (Andrew, Branson, and Wills 1964; Hewish and Okoye 1965), cannot be made to have a direct simple relation to the X-ray production.

We wish to thank the staffs of American Science and Engineering and of the Laboratory for Nuclear Science at Massachusetts Institute of Technology for their assistance throughout this experiment. We are grateful to Dr. Leo Sartori, Professor Philip Morrison, Professor L. Woltjer, and Dr. Oscar Manley for helpful discussions. We are further grateful for the support given us by the staffs of the Sounding Rocket Branch of Goddard Space Flight Center and the White Sands Missile Range. This work was supported in part through funds provided by the National Aeronautics and Space Administration

under contracts NASw-1284 and NASw-1535 and grant NSG-386, and in part by the U.S. Atomic Energy Commission under contract AT(30-1)2098.

M. Oda*
H. Bradt
G. Garmire†
G. Spada‡
B. V. Sreekantan§

February 13, 1967
Massachusetts Institute of Technology
Cambridge, Massachusetts

H. Gursky
R. Giacconi
P. Gorenstein
J. R. Waters

American Science and Engineering, Inc.
Cambridge, Massachusetts

REFERENCES

Allen, R. J., and Barrett, A. H. 1966, presented at 123d meeting of the AAS, Los Angeles (abstract to be published in A.J.).
Andrew, B. H., Branson, N. J. B. A., and Wills, D. 1964, *Nature*, **203**, 171.
Bowyer, S., Byram, E. T., Chubb, T. A., and Friedman, H. 1964, *Science*, **146**, 912.
Gardner, F. F. 1965, *Australian J. Phys.*, **18**, 385.
Gursky, H., Giacconi, R., Gorenstein, P., Waters, J. R., Oda, M., Bradt, H., Garmire, G. and Sreekantan, B. V. 1966*a*, *Ap. J.*, **144**, 1249.
———. 1966*b*, *ibid.*, **146**, 310.
Hewish, A., and Okoye, S. E. 1965, *Nature*, **207**, 59.
Manley, O., and Ouellette, G. 1965 (private communication).
Morrison, P., and Sartori, L. 1967 (in press).
Sandage, A. R., Osmer, P., Giacconi, R., Gorenstein, P., Gursky, H., Waters, J. R., Bradt, H., Garmire, G., Sreekantan, B. V., Oda, M., Osawa, K., and Jugaku, J. 1966, *Ap. J.*, **146**, 316.
Shklovskii, I. S. 1966, *Astr. Zh.*, **43**, 10 (English trans. in *Soviet Astr.—AJ*, **10**, 6, 1966).
Woltjer, L. 1957, *B.A.N.*, **13**, 302.
———. 1964, *Ap. J.*, **140**, 1309.

* Presently at Institute of Space and Aeronautical Science, University of Tokyo, Tokyo, Japan.
† Presently on leave at California Institute of Technology, Pasadena, California.
‡ On leave from the Laboratorio di Astrofisica, Frascati, Italy.
§ Presently at the Tata Institute of Fundamental Research, Bombay, India.

PLATES

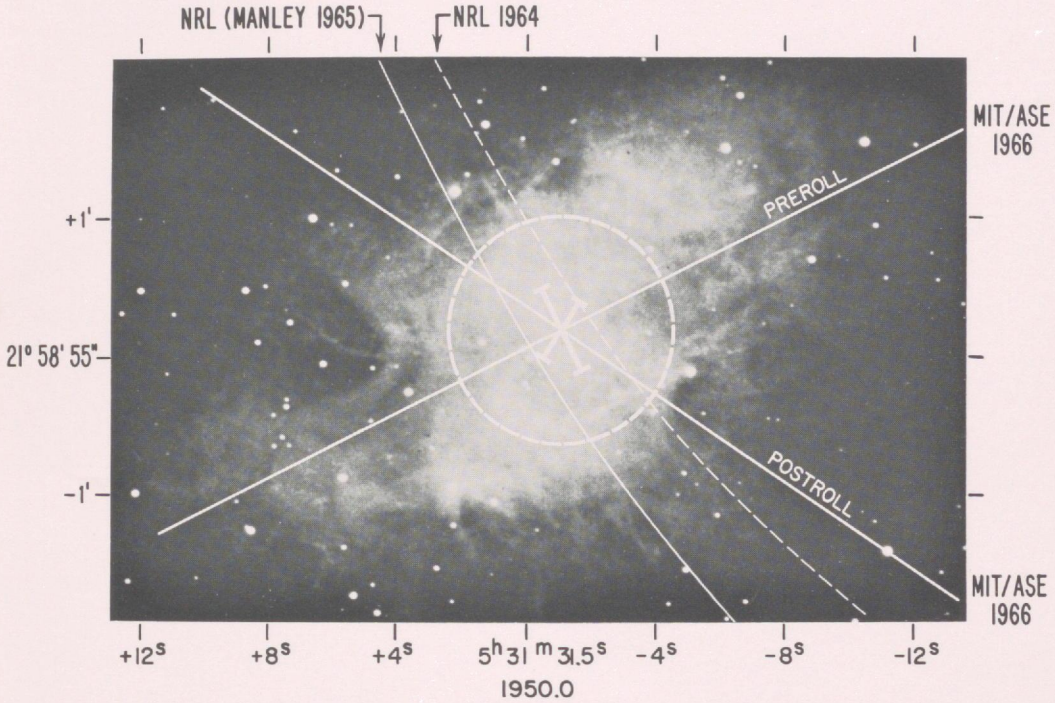

FIG. 5.—Summary of results pertaining to the position of the X-ray source in the Crab Nebula. The dashed curved line is the line of position obtained from a lunar occultation experiment by Bowyer *et al.* (1964), and the solid curved line is the same result corrected by Manley and Ouellette (1965) for parallax due to the motion of the rocket. The intersection of the two MIT/AS&E lines of position is at (1950.0) $\alpha = 5^h\,31^m\,30^s$, $\delta = 21°\,59'.1$. The 100″ diameter circle, taken from Fig. 4, is an idealization of the source region. The origin of the coordinate system is the southwest component of the central double star.

ODA *et al.* (*see* page L9)

The Kolar Gold Fields extensive air shower experiment[1]

B. K. Chatterjee, G. T. Murthy, S. Naranan, K. Sivaprasad, B. V. Sreekantan, A. Suri, and P. R. Viswanath

Tata Institute of Fundamental Research, Bombay, India

Received June 21, 1967

Measurements have been made on high-energy muons (>220 GeV and >640 GeV) in extensive air showers in the size range 10^5–10^7 particles. Results on the energy spectrum, lateral spread (for $E_\mu > 220$ GeV), and the dependence of the total number of muons on the shower size are given. The relation between the number of muons (N_μ) and the shower size (N) can be expressed as

$$N_\mu(>220\text{ GeV}) = 47(N/10^5)^{0.58\pm0.1},$$

$$N_\mu(>640\text{ GeV}) = 4(N/10^5)^{0.77\pm0.2}.$$

Assuming an exponential lateral distribution of high-energy muons, the average lateral spread of muons of energy >220 GeV has been found to be ~40 m.

The results are compared with the predictions of the calculations done by Murthy *et al.* (1967).

The experiment to study the ultra-high-energy (>220 and >640 GeV) muons in extensive air showers has been continued, and further results are presented in this paper.

1. EXPERIMENTAL ARRANGEMENT

The details of the experimental arrangements are given by Chatterjee *et al.* (1966). The basic setup consists of (1) an EAS array of 20 plastic scintillators, each of area 1 m², on the surface, (2) 4 plastic scintillators, each of area 1.5 m², at 270 m depth to detect muons of energy >220 GeV, and (3) 5 water Cerenkov tanks, each of area 2 m², at a depth of 600 m to detect muons of energy >640 GeV. Four low-energy muon (>1 GeV) detectors have been added to the existing array on the surface; these are water Cerenkov tanks, each of area 2 m², and all of them are under a concrete structure which is at a distance of about 10 m from the center of the array. The underground muon detectors provide only "yes" or "no" information.

The recorded events are classified according to the different triggers given by the following selection system:

(*a*) S Trigger: A fourfold coincidence between any four surface scintillators when the recorded density exceeds a preset value of 2 particles/m² for the near detectors (Nos. 1 to 9) and 1 particle/m² for the far-off detectors (Nos. 10 to 19).

(*b*) SU1 Trigger: Coincidence between an air shower pulse from the S trigger and a muon pulse from the 220-GeV level.

(*c*) SU2 Trigger: Coincidence between an air shower pulse and a muon pulse from the 640-GeV level.

(*d*) U_0 Trigger: A fourfold coincidence between pulses from the four low-energy muon detectors corresponding to at least one muon passing through each of the four detectors. This selection system selects showers that are relatively rich in muons.

2. RESULTS

These results are based on about 3 000 hours of operation spread over a period of nine months. About 8 500 SU1 showers, 600 SU2 showers, and 10 000 U_0 showers were recorded. About 8 500 S (unassociated) showers were used for the present analysis. Out of the 8 500 SU1 showers, about 650 showers were associated with two or more muons underground.

All the recorded showers were analyzed using the TIFR CDC3600 computer. For the determination of shower size and core position, the lateral distribution of the density of charged particles in an air shower was assumed

[1]Presented at the Tenth International Conference on Cosmic Rays, held in Calgary, June 19–30, 1967, EAS-5.

to have the form given by the Nishimura–Kamata–Greisen function. Values of the shower size, core position, and age parameter (s) for individual showers were obtained by χ^2-minimization (method of steepest descent). In the present analysis only those showers whose core fell within 50 m from the center of the array and whose probability for detection was nearly unity were accepted.

2.1. Integral Size Spectra

Taking the total running time and the 100% efficient area for detection into consideration, the integral size spectra for all the triggers have been obtained. The values of the exponents of these various spectra are listed in Table I.

TABLE I

Size interval	S	SU1	SU2
10^5–10^6	1.58 ± 0.05	1.13 ± 0.05	0.84 ± 0.16
10^6–10^7	1.80 ± 0.20		

2.2. Absolute Number and Energy Spectrum of Muons

The following method was adopted for the calculation of the number of high-energy muons in a shower of given size.

The rate of arrival of showers of size N in the interval dN from an arrival direction θ within solid angle Ω_1 and core location within an area A_1 is

(1) $$S(N)dN = \int_{\Omega_1}\int_{A_1} F(N)dN \cos^{n+1}\theta \, dA_1 \, d\Omega_1.$$

The density of high-energy muons at a distance r from the axis of the shower is assumed to be given by

(2) $$\Delta(r) = (N_\mu/2\pi r_0^2)e^{-r/r_0}.$$

The rate of association of muons underground with air showers of size N whose cores fall within A_1 on the surface and within A_2 underground is given by

(3) $$SU(N)dN = \int_{A_1}\int_{A_2} F(N)dN \cos^{n+2}\theta \, (1 - e^{-S\Delta}) \, dA_1 \, dA_2/l^2$$

where l is the distance between dA_1 and dA_2 along the shower axis, S is the area of the muon detector, and Δ is the density of muons at the detector when the shower core strikes dA_2. In evaluating the integral, A_1 was restricted to the 100% efficient area of shower detection. Integration with respect to A_2 was carried out over a circle of radius $5r_0$ about the muon detector.

Similarly, the rate of recording muons simultaneously in two detectors underground is given by $SUD(N)dN$, which is the same as $SU(N)dN$ except that the integrand in (3) will contain an additional factor of $(1 - e^{-S\Delta_2})$, where Δ_2 is the muon density at the second muon detector.

The probabilities of singlefold and twofold associations are thus given, respectively, by

$$P_1(N) = SU(N)dN/S(N)dN$$

and $$P_2(N) = SUD(N)dN/S(N)dN.$$

These probabilities were calculated and plotted as a function of N_μ and r_0.

From the experimentally measured fluxes of associated and unassociated showers the probabilities P_1 and P_2 are known. From the calculated plots of these with respect to N_μ and r_0 the latter values are obtained as a function of the shower size.

Figure 1 shows the dependence of the total number of muons of energy >220 GeV and >640 GeV on the shower size in the range 10^5–10^7 particles. The dependence can be expressed by

$$N_\mu(>220 \text{ GeV}) = 47(N/10^5)^{0.58\pm0.1},$$

$$N_\mu(>640 \text{ GeV}) = 4(N/10^5)^{0.77\pm0.2}.$$

Taking a weighted mean slope of $0.62(N_\mu - N_e$ variation) for muons of energy >220 and >640 GeV, the energy spectrum of muons has been obtained as

$$N_\mu(>E, N) = 6.5 \times 10^6(N/10^5)^{0.62}E^{-2.2\pm0.10}.$$

2.3. Arrival Directions

Anisotropy of "mu-rich" showers has been reported by the Tokyo group (Matano *et al.*

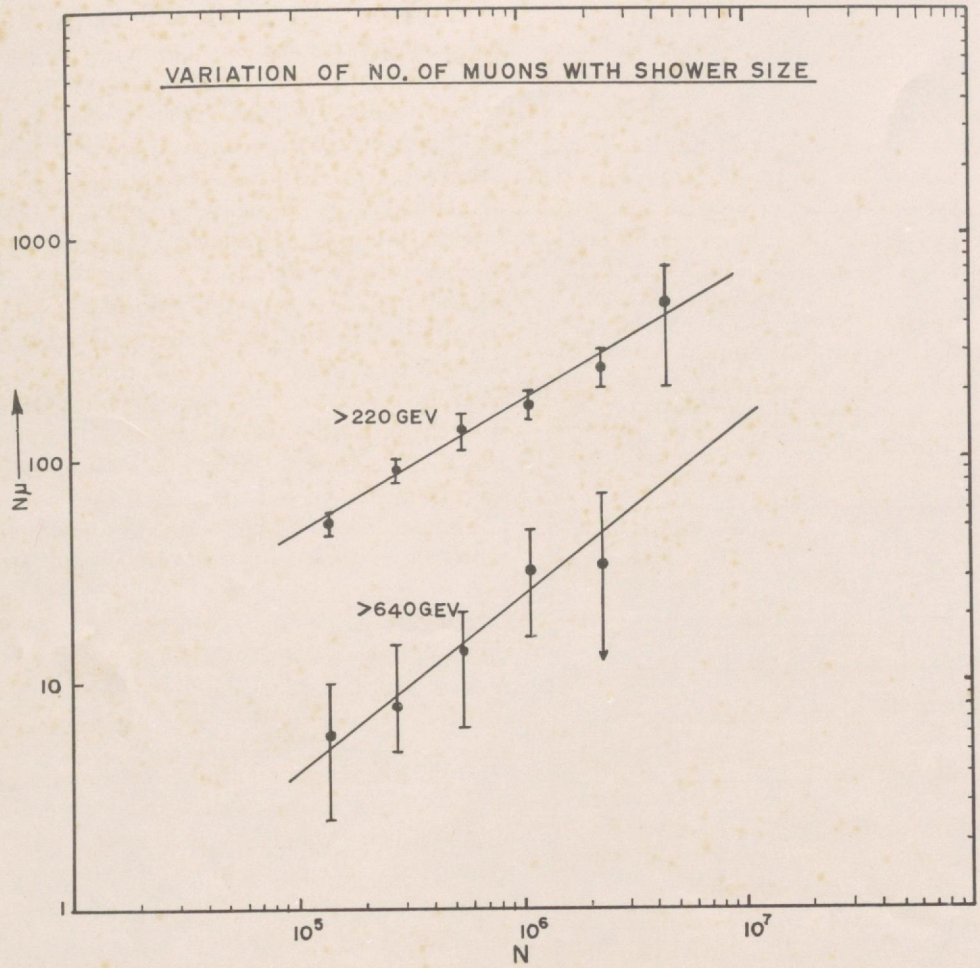

FIG. 1. The variation in the number of muons (>220 and >640 GeV) with shower size.

1966). In the present experiment, the U_0 trigger preferentially picks up showers rich in muons. From the normal U_0 events, a sample of "mu-rich" showers was selected by imposing the following criteria: (*a*) age parameter $s > 1.6$ and (*b*) observed muon density greater than eight times that expected according to the expression given by Greisen (1960). Also it is likely that the showers associated with high-energy muons underground, particularly the multiply associated showers, are rich in high-energy muons. Figure 2 shows the histograms of the number of events in three-hour intervals of sidereal time against sidereal time for SU1 events (single and multiple associations) and U_0 events (normal and "mu-rich"). These plots do not show any statistically significant low or high intensity regions.

3. DISCUSSION

Measurements of the total number of high-energy (>560 GeV) muons have been made by Barrett *et al.* (1952). Their results show that the dependence of the total number of muons on shower size is given by

$$N_\mu(>560\text{ GeV}) \propto N^{0.58\pm0.05}.$$

Greisen (1960), however, gives the following expression for the same experimental data:

$$N_\mu(>560\text{ GeV}) = 75(N/10^6)^\alpha,$$

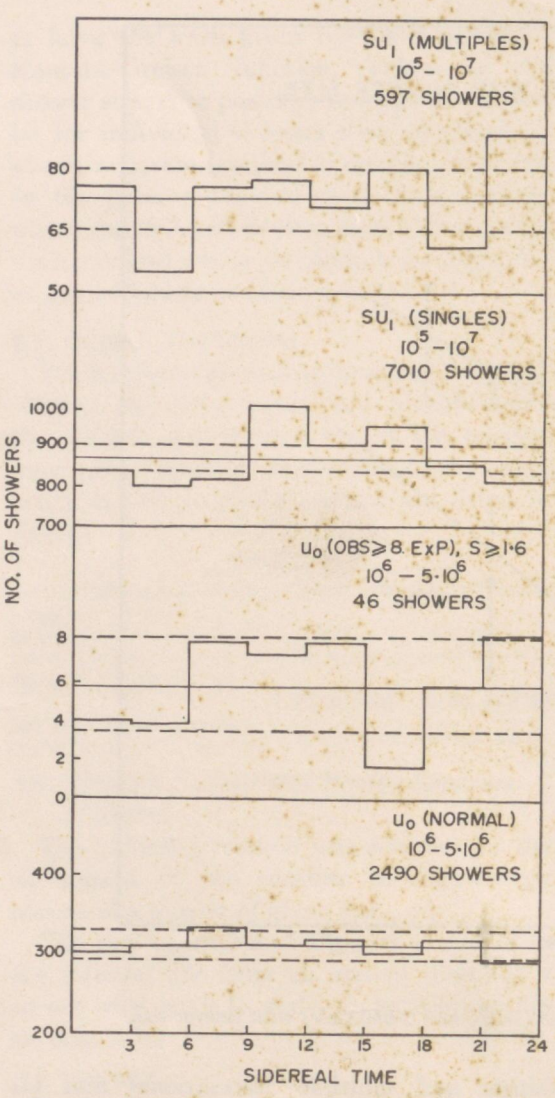

FIG. 2. Arrival directions of air showers rich in muons selected by triggers SU1 and U_0 (see text for explanation).

where $\alpha = 0.7$ for large values of N and N_μ, decreasing towards 0.5 for sizes around 10^3. Although the value of α is in agreement with our results, the above expression gives N_μ larger than obtained in the present experiment. (The difference between our present results and those presented earlier by Chatterjee *et al.* (1966) is probably due to the fact that no strict selection criteria were used in selecting samples of unbiased showers for size distributions in the earlier analysis.)

An estimate of the $\langle p_t \rangle$ of the parents of high-energy muons can be made from the experimentally obtained value of r_0. For muons of energy >220 GeV, we find that r_0 is 20 m with an experimental error of 2–3 m. Monte Carlo calculations, assuming a $\langle p_t \rangle$ of 0.36 GeV/c (Murthy *et al.* 1967), give $r_0 = 11$ m, a value insensitive to most of the models of high-energy interaction used. The experimental value would require a $\langle p_t \rangle$ of 0.6–0.7 GeV/c to be consistent with the calculations.

Comparison of the experimental results with the predictions of Murthy *et al.* (1967) and Lal (1967) shows that it is difficult to decide on any particular model considered by them. All the models predict α ($N_\mu \propto N^\alpha$) in the range of 0.6–0.8, in agreement with our results. However, the total number of muons of energy >220 GeV and their lateral spread, predicted on any model, are smaller than the experimentally obtained values by nearly a factor of two. The discrepancy in N_μ is least in the case of the isobar model without NN production.

ACKNOWLEDGMENTS

Our thanks are due to Sri V. S. Narasimham for his contributions in the early stages of the experiment and to Sri F. Gonsalves, Sri M. P. Kamat, Sri N. R. Manchanda, Sri S. D. Samuel, and Sri A. M. Vinze for their help in the setting up and daily operation of the experiment. The contributions of Smt. N. R. Leelavathi to the analysis of the experimental data are gratefully acknowledged.

REFERENCES

BARRETT, P. H., BOLLINGER, L. M., COCCONI, G., EISENBERG, Y., and GREISEN, K. 1952. Rev. Mod. Phys. **24**, 133.

CHATTERJEE, B. K., LAL, S., MATANO, T., MURTHY, G. T., NARANAN, S., SIVAPRASAD, K., SREEKANTAN, B. V., SRINIVASA RAO, M. V., and VISWANATH, P. R. 1966. Proc. Intern. Conf. Cosmic Rays, London, **2**, 627.

GREISEN, K. 1960. Ann. Rev. Nucl. Sci. **10**, 63.

LAL, S. 1967. Nuovo Cimento, **48A**, 466.

MATANO, T., MIURA, I., NAGANO, M., SHIBATA, S., SUGA, K., and HASEGAWA, H. 1966. Proc. Intern. Conf. Cosmic Rays, London, **2**, 637.

MURTHY, G. T., SIVAPRASAD, K., SRINIVASA RAO, M. V., TONWAR, S. C., VATCHA, R. H., and VISWANATH, P. R. 1967. This Conference, paper EAS-43.

Low-energy muons in extensive air showers at 800 g cm^{-2} [1]

B. K. Chatterjee, N. V. Gopalakrishnan, G. T. Murthy, S. Naranan,
B. V. Sreekantan, M. V. Srinivasa Rao, S. C. Tonwar, and R. H. Vatcha
Tata Institute of Fundamental Research, Bombay, India

Received June 22, 1967

The following results on the low-energy (>0.6 GeV and >1.0 GeV) muons in air showers of size 10^5 to 2×10^7 at Ootacamund (800 g cm^{-2}) are obtained: (1) The average total number of muons $\mathcal{N}_\mu$ varies as $N_e^{0.32\pm0.2}$ for $10^5 < N_e < 10^6$, and as $N_e^{0.8\pm0.15}$ for $10^6 < N_e < 2 \times 10^7$. (2) In showers showing flat electron lateral structure, the $\mathcal{N}_\mu$ variation with N_e is similar to (1). However, in steep showers, $\mathcal{N}_\mu$ varies as $N_e^{0.75\pm0.15}$ in the whole size range 10^5 to 2×10^7. (3) "Muon-rich" showers of size $<10^6$ have less energy in the electron–photon component compared to "normal" showers. No such difference is found for showers of size $>10^6$. (4) There is a slight indication of a deficiency of muon-rich showers having a flat lateral distribution of electrons in the right ascension interval 15–21 hours for showers of size 10^6–10^7. A similar deficit of showers was observed by the Tokyo group for muon-rich showers in the same RA interval.

In this paper, we present the experimental results on low-energy muons, >0.6 GeV and >1.0 GeV, in showers of size 10^5 to 2×10^7 at Ootacamund, (alt 2.2 km, 800 g cm^{-2}). They deal mainly with (A) the average total number of muons as a function of shower size, and (B) the properties of a subsample of specially selected "muon-rich" showers as contrasted with the properties of "normal" showers.

I. EXPERIMENTAL ARRANGEMENT, METHODS OF ANALYSIS

Results for (A) were obtained with an EAS Array (EAS I) consisting of 12 scintillation density detectors spread over a diameter of 80 m, 4 fast scintillators to measure the arrival direction, and 3 muon detectors, each 0.6 m^2, consisting of hodoscoped Geiger counters. Two of the three detectors were shielded by 1.5 m of brick and 2.5 cm of lead up to a zenith angle of 40° and located at 18 and 25 m from the center; the third had 750 g cm^{-2} of iron shielding up to a zenith angle of 30° and was 8 m from the center. The minimum muon energy for penetration was 0.6 and 1.0 GeV in the two cases.

For (B), the results came mainly from an expanded array EAS II (Chatterjee *et al.* 1966*a*), with 20 density detectors, 5 fast scintillators, 4×1.0 m^2 scintillators under 2.5 cm of lead at the center for measurement of the energy density in the soft component, 6×0.36 m^2 scintillators under 2.0 m of water "producer" and 2.5 cm of lead "converter" at the center for energy measurement of N particles, and 4×1.0 m^2 muon detectors, two for >0.6 GeV and two for >1 GeV.

The shower data were analyzed using an electron lateral distribution function $\Delta_e(N, r) \propto N(r/r_0)^{-\alpha_e} \exp(-r/r_0)$, with $r_0 =$ 107 m and a choice of four possible values for α_e, viz. 1.3, 1.5, 1.7, 1.9. The above relation was shown to give a good empirical fit to the experimental results for $r < 50$ m (Chatterjee *et al.* 1964; Chatterjee 1964). For each shower the best set of values of shower core coordinates X, Y, size N, and α_e was determined with an electronic digital computer. At any fixed size N, α_e was found to fluctuate considerably (Chatterjee *et al.* 1964). Errors in X, Y, N, and α_e were estimated by analyzing a large sample of artificial showers generated by the Monte Carlo method; they are about 20% for N, X, and Y, and ± 0.2 for α_e. Details of the procedures of analysis are described by Srinivasa Rao (1967).

[1]Presented at the Tenth International Conference on Cosmic Rays, held in Calgary, June 19–30, 1967, EAS-38.

II. EXPERIMENTAL RESULTS

(A) Variation of the Total Muon Number $\mathcal{N}_\mu$ with Shower Size N

The most direct method of obtaining $\mathcal{N}_\mu$ is to integrate the lateral distribution curves of muon density. In the present experiment, this method raises the following problems: (1) The lateral distributions can be obtained only up to 50 m from the core. Because of systematic errors in the core positions near the periphery of the array, the observed lateral distributions may not reflect true distributions. (2) The statistical errors in core distance measurements near the core ($r < 10$ m) and in density measurements at large distance ($r > 30$ m) are such as to lead to a large error in the integrated value of $\mathcal{N}_\mu(<50$ m). (3) The experimentally determined $\mathcal{N}_\mu(<50$ m) still constitutes only a small fraction of the total $\mathcal{N}_\mu$ in the whole shower.

From experimental work on the lateral distribution of muons it is seen that it is independent of shower size and does not fluctuate appreciably from shower to shower (Greisen 1960; Nikolsky 1963; Matano 1962). Monte Carlo simulations of showers using several different models of high-energy collisions, carried out by us, also lead to the same conclusion. In such a case, it is clear that the error due to (3) is not serious, since $\mathcal{N}_\mu(<50$ m) would be proportional to the total $\mathcal{N}_\mu$. To avoid the sources of error (1) and (2), we adopted the following procedure. Only showers with zenith angle $<30°$ were accepted; the muon detectors were well shielded up to this angle. Two constraints were imposed on core location: the core should be within 25 m from the center to keep the error in the core position low, and it should also be within the interval 15–25 m from the muon detector. This method ensures that the muon density is measured at a mean distance of 20 m in *every* selected shower, a measurement that is subject to least error from all possible sources. This quantity $\Delta_\mu(20$ m) can be regarded as proportional to the total muon number $\mathcal{N}_\mu$, as mentioned above. Throughout the paper, we make this valid assumption: $\Delta_\mu(20$ m) is proportional to $\mathcal{N}_\mu$.

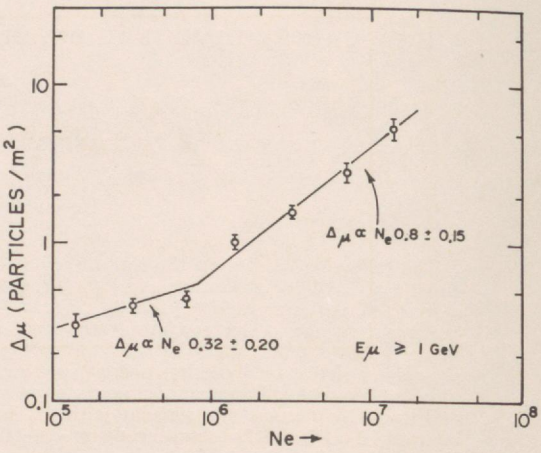

FIG. 1. Variation of muon density at 20 m from shower core, $\Delta_\mu(20$ m), with shower size N_e, for muons of energy >1.0 GeV. It is assumed that $\Delta_\mu(20$ m) is proportional to total $\mathcal{N}_\mu$ (see text).

In Fig. 1 we give the variation of $\Delta_\mu(20$ m) with size for muons of energy >1.0 GeV. Clearly all the points do not fall on a single line; they can, however, be fitted to a straight line of slope 0.3–0.4 for $N < 10^6$, and another line of slope 0.8 for $N > 10^6$ as shown in the figure. A similar change of slope is also seen for muons of energy >0.6 GeV.

We carefully reexamined the data—particularly for $N < 10^6$—to see if triggering biases at low sizes could account for the flattening of the curves below 10^6 in Fig. 1. There are two sources of bias that could favor a biased selection of showers with $\mathcal{N}_\mu$ higher than the average *at low sizes*: (*a*) preferential selection of large zenith angle showers, which have a higher triggering efficiency and also higher $\mathcal{N}_\mu$, and (*b*) biased selection of showers of low α_e at lower sizes, which on experimental evidence (Chatterjee *et al.* 1964, 1966*b*) are correlated with high $\mathcal{N}_\mu$. The effect of (*a*) was found to be small since showers were restricted to a small zenith angle $<30°$, and the threshold density of scintillators used for generating the master shower trigger was kept very low. To assess the contribution of (*b*), showers were reanalyzed defining criteria for $\sim$100% efficient selection, appropriate to

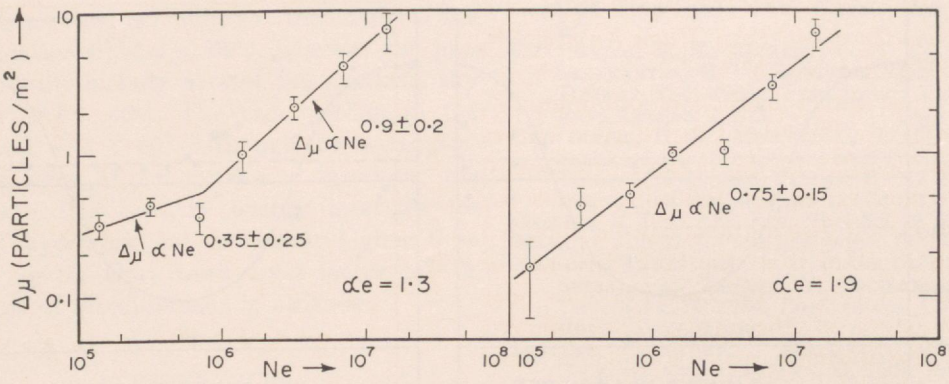

FIG. 2. Variation of $\Delta_\mu(20\text{ m})$ with N_e for muons of energy >1.0 GeV. (*a*) $\alpha_e = 1.3$, "flat" showers. (*b*) $\alpha_e = 1.9$, "steep" showers.

each α_e; it was found that (*b*) could not account for the change in slope for $N < 10^6$.

The higher slope observed for $N > 10^6$ cannot be due to increasing contamination in muon detectors due to N particles and high-energy gamma rays since the contamination is small 20 m from the core. This is further confirmed by the observation that the same behavior is shown in the lower (>0.6 GeV) and higher (>1.0 GeV) threshold detectors.

It is therefore concluded that the observed variation of $\Delta_\mu(20\text{ m})$ with shower size reflects a *genuine physical change of slope in the relation* $\mathcal{N}_\mu \propto N^\beta$ *with* β *changing from a low value of* ~ 0.3 *for* $N < 10^6$ *to a higher value of 0.8 for* $N > 10^6$, *rather sharply at* $N \sim 10^6$. We believe that such a change was not noticeable in earlier work (Chatterjee *et al.* 1964) because of the large experimental and possible systematic errors involved in obtaining $\mathcal{N}_\mu(<50\text{ m})$ by integrating the lateral distributions as discussed above.

Our observations have shown that α_e is a physically meaningful shower parameter in addition to the shower size (Chatterjee *et al.* 1964, 1966*b*). It would be interesting to see the behavior of the $\mathcal{N}_\mu$–N curve for different values of α_e. In Fig. 2 (*a*) and (*b*), we show the results for >1.0 GeV muons, and for $\alpha_e = 1.3$ and 1.9 respectively. The "flat" showers ($\alpha_e = 1.3$) show the same behavior of a change in slope at $N = 10^6$ as in Fig. 1. However, for "steep" showers ($\alpha_e = 1.9$) there appears to be no such change of slope, the slope being consistent with a single value 0.75 in the whole size range 10^5 to 2×10^7. Although the statistical significance of this observation needs to be improved, the difference in curves of Fig. 2 (*a*) and (*b*) is striking. A similar difference is also seen for muons of energy >0.6 GeV. The dependence of β on α_e at low sizes would also imply that if all showers are analyzed assuming an invariant lateral distribution of electron density (constant α_e), any real change of β with size might escape observation.

(*B*) *Properties of "Muon-Rich" Showers*

At the London Conference, we presented the results on the differences in the properties of showers selected by (1) the usual electron trigger and by (2) a muon trigger, requiring $\geqslant 1$ muon in each of four widely separated muon detectors, with no constraint on electron density (Chatterjee *et al.* 1966*a*). The "muon-triggered" showers were also "muon-rich" in the lower size group of 10^5–10^6, whereas they were similar to "normal" showers for the higher size group 10^6–10^7. The main results were: (1) for showers of size 10^5–10^6, the muon-rich showers had much less energy in the electron–photon and N components in the core region (<5 m) compared to normal showers; (2) their arrival directions were also uniformly distributed in right ascension just like normal showers. In that

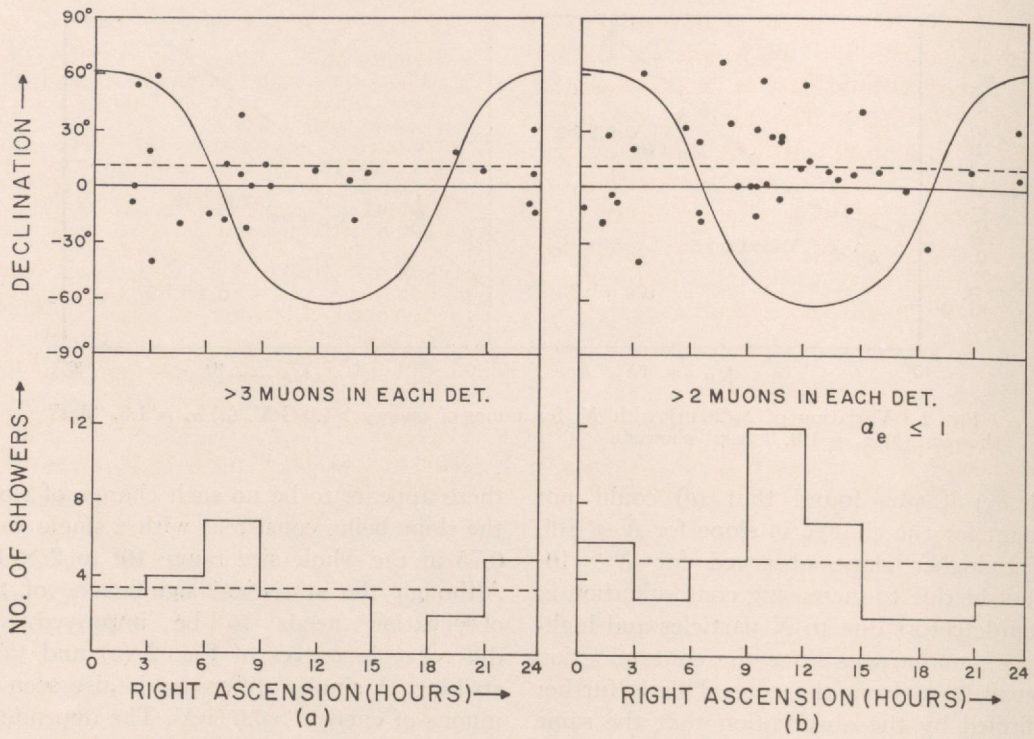

FIG. 3. Celestial plot of arrival directions of "muon-rich" showers of size 10^6–10^7 at Ootacamund (11 °N, 2.2 km) with different criteria for (*a*) and (*b*).

paper, no conclusion could be drawn about the properties of muon-rich showers in the size range 10^6–10^7.

Here, we report on the distribution of shower arrival directions for a group of showers of size 10^6–10^7 selected by using suitable criteria of "muon-richness". We found that by demanding more than three muons in each of the four muon detectors, we select 10^6–10^7 showers which have $\mathcal{N}_\mu$ about 2–3 times the average value. In Fig. 3(*a*), the shower directions are shown on a Mercator projection of the celestial sphere at the top, and as a frequency distribution in 3-h right ascension intervals at the bottom. An alternative criterion was also used (>2 muons in each of 4 detectors, *and* $\alpha_e \leqslant 1.0$), and the results are shown in Fig. 3(*b*). To ensure uniform exposure in right ascension, only data that accumulated continuously over 24-hour periods were used. There were 21 such 24-hour periods.

In Fig. 3(*b*) there is an apparent decrease in the number of showers in the 15–21 hour interval which could be due to statistical fluctuation. However, a chi^2 test gives only a probability of $<3\%$ that the observed distribution is consistent with the hypothesis of a uniform distribution. This observation becomes specially significant when it is noted that the Tokyo group (Matano *et al.* 1966) observed a similar "dark region" for muon-rich showers of size 10^6–10^7 at sea level in the same right ascension interval of 15–21 hours. Also, the two experiments did not show any evidence for nonuniform distribution in RA for "normal" showers in the whole size range 10^5–10^7, and also for "muon-rich" showers of the lower size group 10^5–10^6 (Chatterjee *et al.* 1966*a*, Matano *et al.* 1964). The similarity of the two observations is striking particularly since the two experiments were conducted at different latitudes (Tokyo 36 °N, Ooty 11 °N) and with different muon detectors. The Tokyo

results are confined mainly to the northern sky (declination $6° < \delta < 66°$), whereas the present results include part of the southern sky ($-20° < \delta < 40°$). The two overlap in the region $6° < \delta < 40°$. Although the two experiments refer to the same size intervals, the corresponding primary energy intervals for the Tokyo work are somewhat higher than those for the Ooty work, by a factor of ~ 2, because of the difference in altitude.

REFERENCES

CHATTERJEE, B. K. 1964. Ph.D. thesis, Bombay University.

CHATTERJEE, B. K., MURTHY, G. T., NARANAN, S., SREEKANTAN, B. V., and SRINIVASA RAO, M. V. 1964. Proc. Intern. Conf. Cosmic Rays, Jaipur, **4**, 227.

CHATTERJEE, B. K., MURTHY, G. T., NARANAN, S., SREEKANTAN, B. V., SRINIVASA RAO, M. V., and TONWAR, S. C. 1966*a*. Proc. Intern. Conf. Cosmic Rays, London, **2**, 635.

CHATTERJEE, B. K., MURTHY, G. T., NARANAN, S., SREEKANTAN, B. V., SRINIVASA RAO, M. V., TONWAR, S. C., and VATCHA, R. H. 1966*b*. Proc. Intern. Conf. Cosmic Rays, London, **2**, 635.

GREISEN, K. 1960. Ann. Rev. Nucl. Sci. **10**, 63.

MATANO, T. 1962. J. Phys. Soc. Japan, **17**, 745.

MATANO, T., MIURA, I., NAGANO, M., ODA, M., SHIBATA, S., TANAKA, Y., TANAHASHI, G., and HASEGAWA, H. 1964. Proc. Intern. Conf. Cosmic Rays, Jaipur, **4**, 248.

MATANO, T., MIURA, I., NAGANO, M., SHIBATA, S., SUGA, K., and HASEGAWA, H. 1966. Proc. Intern. Conf. Cosmic Rays, London, **2**, 637.

NIKOLSKY, S. I. 1963. Soviet Phys. Usp. English Transl. **5**, 849.

SRINIVASA RAO, M. V. 1967. Ph.D. thesis, Bombay University.

High-energy N particles in extensive air showers at 800 g/cm

B. K. Chatterjee, G. T. Murthy, S. Naranan, B. V. Sreekantan,
M. V. Srinivasa Rao, S. C. Tonwar, and R. H. Vatcha

High-energy N particles in extensive air showers at 800 g/cm²[1]

B. K. Chatterjee, G. T. Murthy, S. Naranan, B. V. Sreekantan,
M. V. Srinivasa Rao, S. C. Tonwar, and R. H. Vatcha
Tata Institute of Fundamental Research, Bombay, India

Received June 25, 1967

The results on high-energy N particles in EAS using a total absorption spectrometer for energy measurement are presented. They are compared with results from other experiments and calculations based upon plausible models of high energy interactions. (1) As expected, the NAP lateral distribution becomes steeper for particles of higher threshold energies. (2) Contrary to expectation, the lateral distribution becomes flatter with increasing shower size. The implication of this anomalous behavior in terms of interaction characteristics at energies $>10^{14}$ eV is briefly discussed. (3) For a given size, showers with steeper electron lateral distribution have more NAPs. (4) Except for the behavior of the lateral distribution as a function of size, all the other results can be explained in terms of models in which p_T and inelasticity distributions are invariant and some fraction ($\sim$15%) of nucleon–antinucleon pair production is assumed.

INTRODUCTION

The N component of energies $\geqslant$50 GeV has been studied in EAS using a total absorption spectrometer (TAS) (Ramana Murthy *et al.* 1963). The air showers are triggered by an electron density criterion (Murthy 1967). All the showers are classified into groups of nearly the same size N_e, electron lateral structure parameter α, and distance r of shower axis from the TAS. Only showers with core distance $<$10 m from the center were accepted; the error in core position was 1–2 m in individual showers. The TAS used here estimates* the energy quite reliably as (1) it is insensitive to interaction characteristics, (2) it is shielded well against electron contamination, and (3) its geometry is well defined since only showers incident at zenith angles $<20°$ are accepted. The uncertainty in the energy estimate is $\leqslant$40%.

LATERAL DISTRIBUTIONS

The density ρ_n of NAPs of any threshold energy E for showers of any (N_e, α, r) group has been determined by the "inefficiency" method, from the fraction of events in which no particle was recorded. The lateral distributions are well represented by an exponential function defined by

$$(1) \qquad \rho_n(N_e, r, >E) = A \exp(-r/r_0),$$

where A, the density in the core, is given by

$$(2) \qquad A = 8.2(N_e/2 \times 10^7)^{0.097E^{0.28}}$$

and r_0, the lateral distribution parameter, is given by

$$(3) \quad r_0 = 13.3(N_e/2 \times 10^7)^{0.39-0.049E^{0.28}} \times (E/50)^{-0.55}$$

for $0 \leqslant r \leqslant 15$ m, $50 \leqslant E \leqslant 1\,600$ GeV, and $3 \times 10^4 \leqslant N_e \leqslant 3 \times 10^6$.

Figure 1 shows the lateral distributions of NAPs ($>$50 GeV) for showers of different sizes irrespective of the α value. Figure 2 shows that r_0 increases with size. It can also be seen that as the energy threshold increases, this dependence weakens. For a given size group, the lateral distributions steepen with increase in threshold energies as shown in Fig. 3. Power laws with positive and negative exponents can be fitted to the variation of r_0 with size and threshold energies respectively as expressed by eq. (4), which is obtained from eqs. (1), (2), and (3):

$$(4) \qquad N_n(>E, N_e) = 1.75N_e^{0.78}E^{-1.1}.$$

Within the statistical errors any correlation between fluctuations in α and r_0 is weak.

[1]Presented at the Tenth International Conference on Cosmic Rays, held in Calgary, June 19–30, 1967, EAS-39.

*The TAS energy estimate as given here has to be corrected by 40% to take into account energy not absorbed in the TAS.

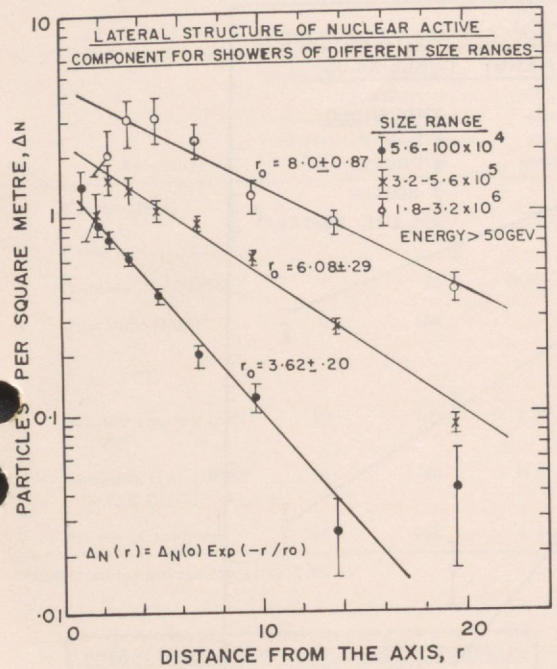

FIG. 1. Lateral distribution of NAPs (>50 GeV).

ENERGY SPECTRUM

The integral energy spectrum is obtained by integrating the fitted lateral distribution function for each energy threshold. Figure 4 shows that the integral energy spectrum exponent increases with increasing energy for the same distance group and with increasing distance for the same energy group. Figure 5 shows that the integral energy spectrum for all NAPs in a shower can be fitted to a negative power law of the same exponent independent of size. Again within errors, there is only a slight trend for correlation between fluctuations in α and the exponent of the integral energy spectrum.

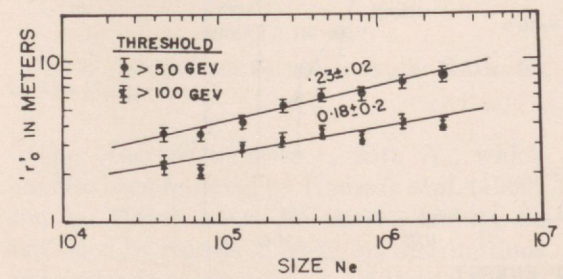

FIG. 2. Variation of r_0 with size.

NUMBER OF NAPs

Figure 6 indicates the extent of the correlation between the fluctuation in the total number of NAPs per shower N_n and α, at a fixed size; the increase of N_n with N_e can be fitted to a power law. Figure 7 shows that when summed up for all α, this exponent is independent of threshold energies. Systematically higher values of N_n at low N_e may be due to residual selection bias.

SUMMARY

The main results are:

(1) The average integral energy spectrum $\propto E^{-1.1}$ for all size groups, and the size variation of the total number of NAPs N_n per shower $\propto N_e^{0.78}$.

(2) r_0 increases with size N_e and decreases with threshold energy E as expressed in eq. (3).

(3) For a given size, showers with steeper electron lateral distribution have more NAPs.

DISCUSSION

Table I gives a comparative study of the results obtained by different workers on NAPs in air showers. The difference in the slope of the integral energy spectrum as obtained from the present experiment compared to values from other experiments could possibly arise from the method used in processing showers. In the present experiment α is a free parameter fitted to the observed lateral distribution. A fixed structure function could result in a different estimation of N_e in individual showers. Discrepancies in the number of NAPs and their size variation exponent could arise from systematic errors in energy estimates, detectors used, and effects of altitude variation.

The integral energy spectrum and the size variation of NAPs can be explained by all plausible models considered (Murthy *et al.* 1967). However, the absolute number of NAPs obtained in the present experiment can be explained only by models in which nucleon–antinucleon production occurs in high-energy interactions.

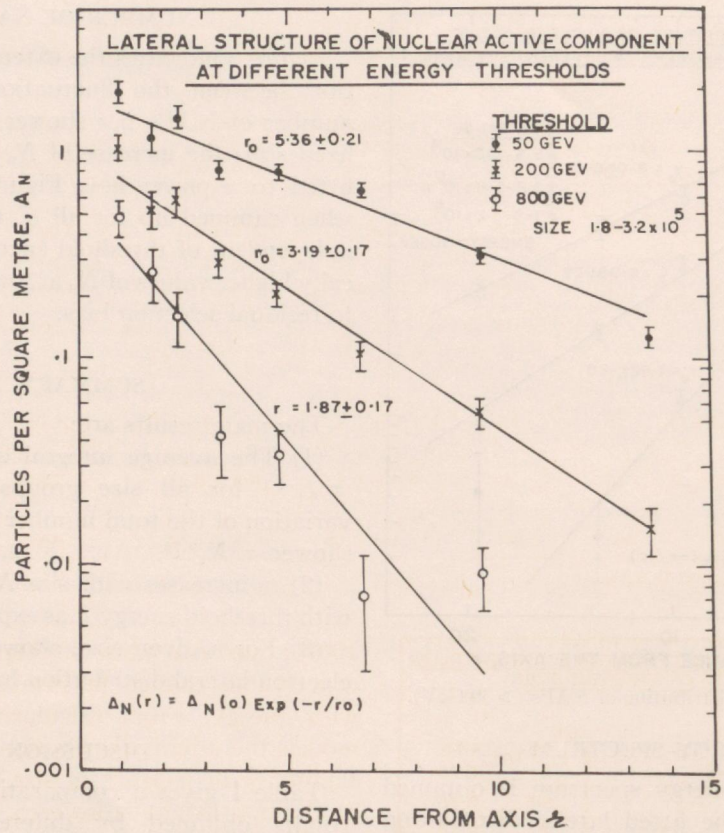

FIG. 3. Lateral distribution of NAPs for various threshold energies.

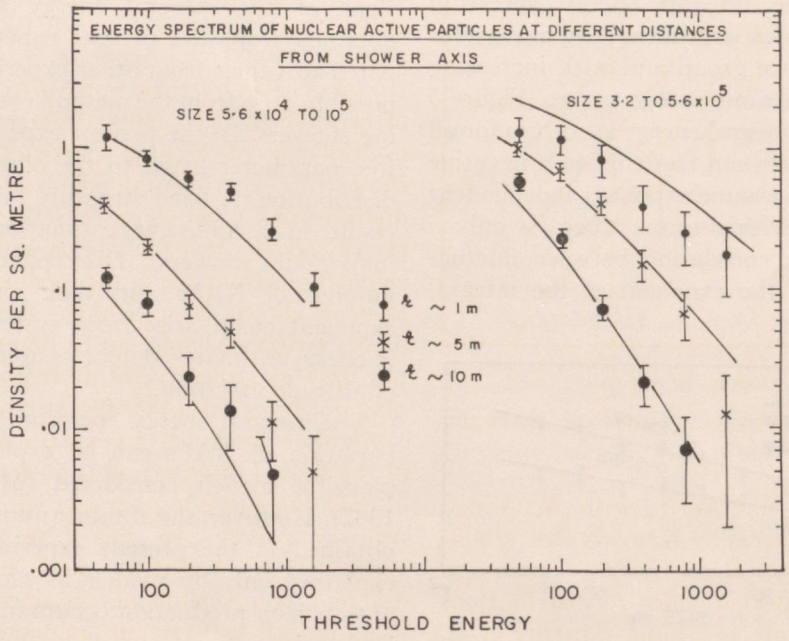

FIG. 4. Integral energy spectrum of NAPs for various distance groups.

TABLE I

No.	Reference	No. of NAPs of energy >100 GeV: Shower size (10^5)	No. of NAPs of energy >100 GeV: Shower size (10^6)	Slope of integral energy spectrum	Exponent of size variation	Altitude of observation (g/cm²)	Detector
1	Tanaka (1961)	50	625	1.0 ± 0.1	1.1 ± 0.1	1 000	Transition chamber
2	Fukui *et al.* (1960)						
3	Kameda *et al.* (1966)	7.2	72	0.75 ± 0.1	1.0 ± 0.1	1 000	Cloud chamber
4	Tanahashi (1965)	9	110	1	1.1	1 000	Pb glass Cerenkov underground scintillator
5	Nikolski's survey (SIN) (1963)	10	100	1.0 ± 0.1	1.0	All altitude data combined	Different detectors
6	Hasegawa *et al.* (1966) BASJE (HNS)	10	80	0.9 ± 0.1	0.8 ± 0.1	530	Lead-shielded scintillators
7	Present experiment*	105	630	1.1 ± 0.05	0.78 ± 0.05	800	TAS

*Corrected for leakage energy in TAS.

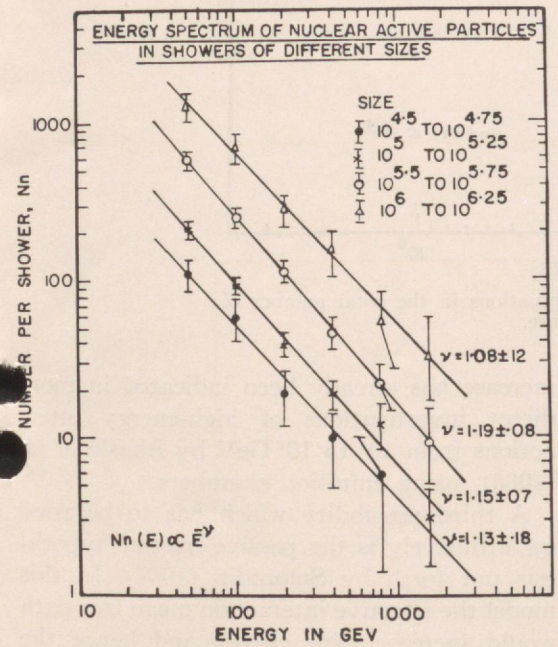

FIG. 5. Integral energy spectrum of NAPs for various size groups.

The observed increase r_0 with N_e, which has also been reported by Kameda *et al.* (1966) and by Hasegawa *et al.* (1966), cannot be explained by models in which p_T distributions and inelasticity are invariant (Murthy *et al.* 1967); nor can this be explained by any conceivable change in primary composition with energy. From calculations using such models the lateral distribution should steepen slightly with increase in size as the effective production height is lowered. To understand the flattening, a preliminary calculation based on a model with the following changes in interaction characteristics above 10^5 GeV was tried (Murthy 1967): (i) increase in inelasticity, (ii) increase in average transverse momentum of created particles, (iii) a faster increase in multiplicity of created particles. Figure 8 shows the experimental points of the lateral distributions together with results from the above model. Also for comparison results of calculations from one of the models of Murthy *et al.* are shown. In spite of the agreement, the model assumed should not be taken as unique, but only as indicative of a trend. As such it may not bring out other features of EAS.

Another possibility to explain the behavior of the lateral distribution is an increase in p_T of only the surviving particle with increasing primary energy. In this case the energy spectra, size variation, and numbers of different components as obtained from the usual models will remain unaffected. Such an

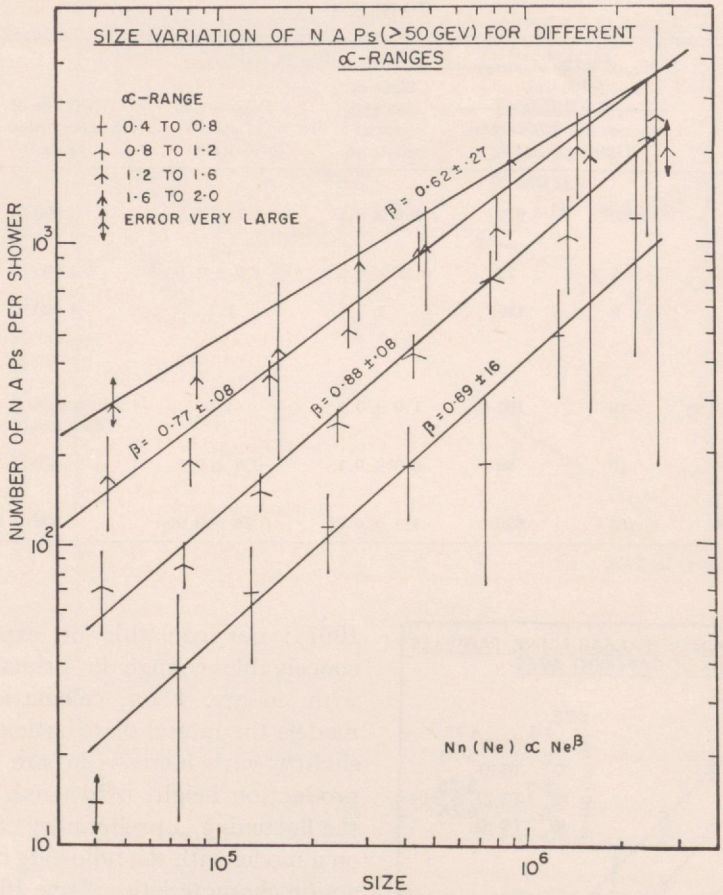

FIG. 6. Correlations between fluctuations in the total number of NAPs and the electron lateral structure.

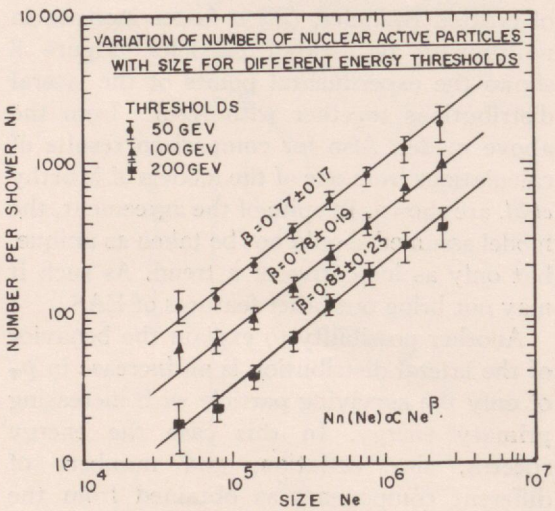

FIG. 7. The variation of the number of NAPs with size for various threshold energies.

increase has already been indicated in more direct investigations of high-energy interactions from 10^5 to 10^6 GeV by Akashi *et al.* (1966), using emulsion chambers.

A third possibility which has to be tried quantitatively is the passive baryon hypothesis put forth by Smorodin (1967). In this model the effective interaction mean free path would increase with energy and hence the effective production height of NAPs of a given threshold energy at a given level will increase with primary energy. Thus, besides explaining the flattening of the lateral distribution of NAPs with increasing size, it may also explain the very broad distribution in α at sizes exceeding 10^6 which has been reported by Murthy (1967).

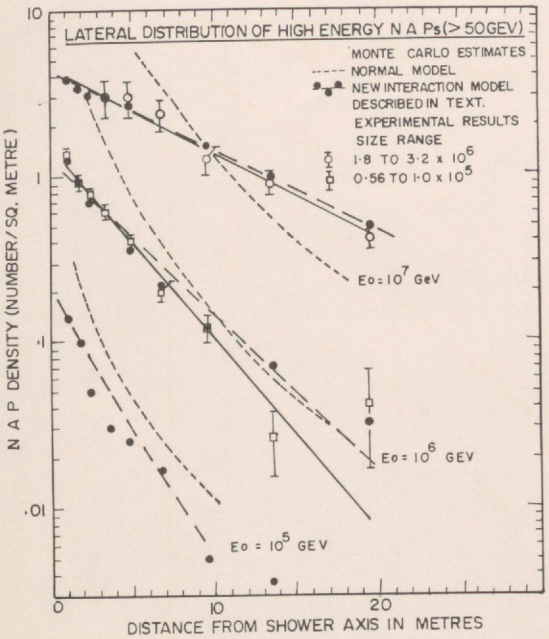

FIG. 8. Calculated lateral distributions of NAPs for various size groups.

REFERENCES

AKASHI, M. *et al.* (Japanese and Brazilian Emulsion Groups). 1966. Proc. Intern. Conf. Cosmic Rays, London, **2**, 835.

FUKUI, S., HASEGAWA, H., MATANO, T., MIURA, I., ODA, M., SUGA, K., TANAHASHI, G., and TANAKA, Y. 1960. Progr. Theoret. Phys. Kyoto, Suppl. **16**, 1.

HASEGAWA, H., NOMA, M., SUGA, K., and TOYODA, Y. 1966. Proc. Intern. Conf. Cosmic Rays, London, **2**, 642.

KAMEDA, T., MAEDA, T., ODA, H., and SUGIHARA, T. 1966. Proc. Intern. Conf. Cosmic Rays, London, **2**, 681.

MURTHY, G. T. 1967. Ph.D. thesis, Bombay University (unpublished).

MURTHY, G. T., SIVAPRASAD, K., SRINIVASA RAO, M. V., TONWAR, S. C., VATCHA, R. H., and VISWANATH, P. R. 1967. This Conference, paper EAS-44.

NIKOLSKI, S. I. 1963. Soviet Phys. Usp. English Transl. **5**, 849.

RAMANA MURTHY, P. V., SREEKANTAN, B. V., SUBRAMANIAN, A., and VERMA, S. D. 1963. Nucl. Instr. Methods, **23**, 245.

SMORODIN, YU. A. 1967. Soviet Phys. JETP English Transl. **24**, 290.

TANAHASHI, G. 1965. J. Phys. Soc. Japan, **20**, 883.

TANAKA, Y. 1961. J. Phys. Soc. Japan, **16**, 866.